Physica C: Superconductivity and its applications 531 (2016) 93–97

Contents lists available at ScienceDirect

Physica C: Superconductivity and its applications

journal homepage: www.elsevier.com/locate/physc

Characterization of the Nb-B superlattice system

D.G. Franco, A. Sarmiento-Chavez, N. Schenone[2], A.E. Llacsahuanga Allcca[1], M. Gómez Berisso, Y. Fasano, J. Guimpel*

Comisión Nacional de Energía Atómica - Centro Atómico Bariloche, Instituto Balseiro - Universidad Nacional de Cuyo, and CONICET, 8400 Bariloche, Río Negro, Argentina

ARTICLE INFO

Article history:
Received 7 September 2016
Revised 21 October 2016
Accepted 2 November 2016
Available online 3 November 2016

Keywords:
Superlattice
Superconductivity
Transition edge sensors

ABSTRACT

We study the growth, stacking and superconducting properties of Nb and B thin films and superlattices. The interest in these resides in their possible use in transition edge neutron sensors. The samples were grown by magnetron sputtering over Si (1 0 0) substrates. The X-ray diffraction patterns for all Nb containing samples show a Nb (1 1 0) preferential orientation. From the low-angle X-ray reflectivity we obtain information on the superlattice structure. The superconducting transition temperatures of the superlattices, obtained from the temperature dependence of the magnetization, are higher than those of single Nb films of similar thickness. The temperature dependence of the perpendicular and parallel upper critical fields indicate that the superlattices behave as an array of decoupled superconducting Nb layers.

1. Introduction

Radiation and particle detection rely on a broad range of detector types based in a wide range of physical phenomena. Among these, the transition edge sensors (TES) rely on a sharp thermodynamic phase transition triggered by the local heating due to the capture of an energy quantum or a particle [1]. In particular, a superconducting transition, with a very sharp electrical resistance change between a finite value and zero, offers a simple detection method from voltage vs. time measurements. Another type of detectors based on superconducting materials are the Kinetic Inductance Detectors (KID) [2], where a change in the kinetic inductance of the superconductor is originated by the unpairing of Cooper pairs produced by the absorption of the detected radiation.

Superconductivity up to relatively-high temperature in MgB_2, [3] has attracted attention for its possible use in a superconducting TES [4,5] and KID [6] for detection of thermal neutrons. In effect, ^{10}B presents a large cross section for the capture of thermal neutrons, 3840 barn, together with a natural 20% abundance. The products of the $^{10}B(n,\alpha)^7Li$ reaction share 2.31 MeV which can produce local heating if this energy is absorbed by the material, which is usually the case, given the short stopping ranges of 1.9 µm for ^7Li and 3.8 µm for α particles. However, MgB_2 has proved to be a difficult material for thin-film deposition, usually requiring of high deposition temperatures, making its use incompatible for integration in semiconductor devices.

As an alternative regarding the use in TES, it is not necessary for the B atoms to be part of the actual crystalline structure of the superconductor. The material could be a composite material of B and a superconductor thin film. One possibility for the superconducting material is Nb, with a bulk superconducting critical temperature (T_c) of 9.26 K. This motivated us to study the Nb/B superlattice system for a possible use in TES design. Here we focus on the study of the material itself. The phase diagram of the Nb-B binary alloy shows the existence of different compounds, [7] which could enhance diffusion at the interfaces, giving rise to non superconducting phases and precluding the formation of the superlattice system. The artificial periodicity of the superlattice structure allows to study the interface structure through X-Ray diffraction and reflectivity. We will show that interdiffusion at the interfaces is not precluding the superlattice growth or degrading the superconducting properties and that Nb/B superlattices are a potential candidate for the design of a position sensitive neutron TES. Recently, Ishida et al. [8,9] have presented results on a Nb/^{10}B/Nb trilayer KID showing the feasibility of these detectors.

2. Material and methods

Thin films and superlattices were grown at room temperature by magnetron sputtering from >99.9% pure Nb and B targets on

* Corresponding author.
E-mail address: jguimpel@cab.cnea.gov.ar (J. Guimpel).
[1] Present address: Department of Physics and Astronomy, Purdue University, USA.
[2] Permanent address: Physique-Nanosciences, Phelma, Grenoble INP, France.

http://dx.doi.org/10.1016/j.physc.2016.11.002
0921-4534/

Table 1
Identifying labels for each superlattice. Labels take the form $(Nbd_{Nb}/Bd_B)_{\times N}$ with d_{Nb} and d_B the nominal layer thicknesses in nm, and N the number of periods.

	d_B				
d_{Nb}	5 nm	10 nm	15 nm	20 nm	30 nm
5 nm	$(Nb5/B5)_{\times 10}$	$(Nb5/B10)_{\times 6}$	–	–	–
10 nm	$(Nb10/B5)_{\times 6}$	$(Nb10/B10)_{\times 5}$	$(Nb10/B15)_{\times 4}$	–	–
15 nm	–	$(Nb15/B10)_{\times 4}$	$(Nb15/B15)_{\times 4}$	–	–
20 nm	–	$(Nb20/B10)_{\times 3}$	–	$(Nb20/B20)_{\times 3}$	–
30 nm	–	$(Nb30/B10)_{\times 3}$	–	–	$(Nb30/B30)_{\times 3}$

Si (100) substrates in a 10 mTorr Ar atmosphere. Nb was deposited by dc sputtering, while rf sputtering was used for B. Deposition rates were calibrated by measuring the thickness of Nb or B thin films grown for different total deposition times. In addition, the thickness of all the studied films was measured by contact perfilometry in a well-defined sample edge. This edge was generated by first masking part of the substrate with silver epoxy, growing the film, and finally removing the epoxy. For the Nb films total thickness was also measured by small angle X-Ray reflectometry (XRR), as will be explained in the next section. Both methods showed consistent results. The determined deposition rates for the adopted growth conditions were ~1.6 nm/s for Nb and $\sim 2.6 \times 10^{-2}$ nm/s for B.

Table 1 summarizes the superlattices used in this study with different Nb and B layer thicknesses. The number of periods was adjusted for the total thickness of each superlattice to be as close as possible to 100 nm. Growth was always started with a Nb layer and, consequently, ended with a B layer. With this set of samples we were able to study the systematics for equal Nb and B layer thickness (diagonal in the table), for constant B thickness (columns in the table) and for constant Nb thickness (rows in the table).

Superlattices $(Nb10/B20)_{\times 3}$ and $(Nb10/B30)_{\times 3}$ were also grown but repeatedly resulted in a highly tensioned material that easily and spontaneously peeled off from the substrate. We believe this is probably a consequence of the large mismatch between B and Nb elastic constants, inducing a large stress for thick B layers over relatively thin Nb layers. A study of the mechanical properties of the superlattices is under way and will be published elsewhere.

The crystalline structure of the samples was analyzed by X-Ray diffraction (XRD) patterns at high angles and XRR at low angles. Stacking, quality, and thickness of the layers were studied from low angle XRR. The difractograms were measured at room temperature on a PANalytical Empyrean diffractometer in Bragg–Brentano geometry with Cu K_α radiation, wavelength $\lambda = 1.5418$ Å. Samples were mounted in a 4-circle Eulerian cradle, which allowed for precise alignment of the sample.

The superconducting properties were studied through magnetization and electrical transport measurements. Temperature (T) and magnetic field (H) dependence of the magnetization (M) were measured in a commercial SQUID magnetometer with H perpendicular to the sample surface. M vs T was measured between 5 and 11 K both for zero field cooling (ZFC) and field cooling (FC) protocols.

Electrical resistance (R) as a function of T was measured for constant H. All samples were patterned in a four terminal configuration bar 1 mm long and 5 μm wide using electron beam lithography and chemical etching. H was applied with an external electromagnet which allowed rotation of its direction around a vertical axis. Critical superconducting upper fields were determined for fields both perpendicular ($H_\perp$) and parallel ($H_\parallel$) to the surface of the samples, with the electrical current always perpendicular to H.

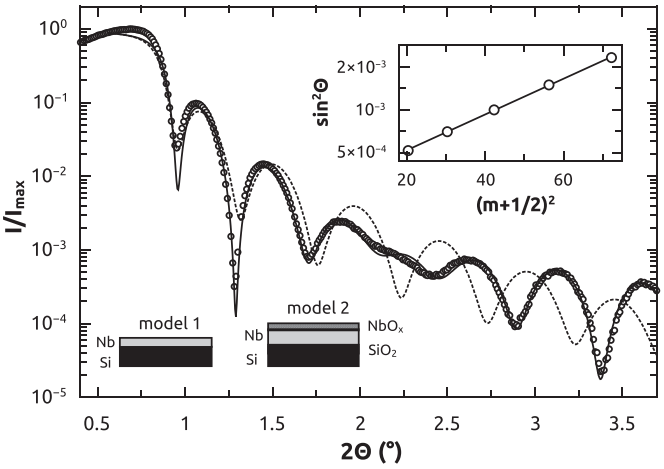

Fig. 1. Low angle X-ray reflectivity for a 17 nm thick Nb thin film. Open circles: experimental data; dotted line: fit with a model consisting of a Nb layer over the Si substrate (model 1); continuous line: fit with a model including a SiO_2 layer at the Si/Nb interface and a NbO_x layer at the film surface (model 2). The inset shows the peak position vs. order number. Open circles: experimental data; line: linear fit. See text for details.

3. Results and discussion

3.1. Crystalline structure of Nb thin films and Nb/B superlattices

The high angle XRD diffraction patterns for the Nb thin films indicate textured growth. Besides the Si (400) reflection at $2\theta = 69.196^\circ$ we found two additional reflections corresponding to the (110) family of planes for bcc Nb. The lattice parameter is in all cases very close to that for bulk Nb, $a = 3.3066$ Å(JCPDF 35-0789). Concerning the structure and texture of B thin films, no diffraction peaks were observed at high angles due to the small X-Ray scattering factor for this element.

Fig. 1 shows the low angle XRR curve for a 17 nm thick Nb thin film. Qualitatively, the curve shows the expected behavior. In the first place, total reflection below a critical angle of $2\Theta \approx 0.75^\circ$ is clearly seen, close to twice the expected critical angle $\alpha_c = 0.398^\circ$ for bulk Nb [10]. This originates in the fact that the X-Ray index of refraction of a material, $n = 1 - \delta$, with δ proportional to the electronic density, is smaller than that of vacuum. Second, Kiessig fringes due to the finite thickness of the film are clearly observed [11]. For the case of a substrate with lower electronic density than the film material, the intensity maxima are expected to appear at [12]

$$\sin^2\theta = \left(m + \frac{1}{2}\right)^2 \left(\frac{\lambda}{2e}\right)^2 + 2\delta \qquad (1)$$

where $m \geq 0$ is an integer, λ the X-Ray wavelength and e the thickness of the film. The experimental data seems to follow this law

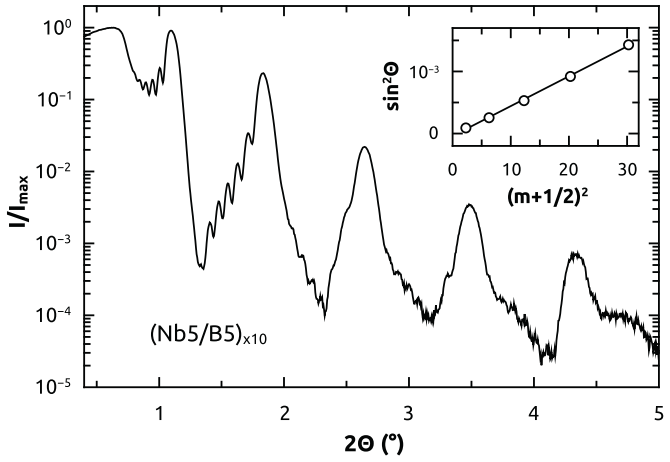

Fig. 2. Low angle X-ray reflectivity for a $(Nb5/B5)_{\times 10}$ superlattice. Kiessig fringes [11] due to total thickness and superlattice diffraction peaks are clearly observed. The inset shows the linear dependence between $sin^2\Theta$ and $\left(m+\frac{1}{2}\right)^2$ for the superlattice diffraction peaks.

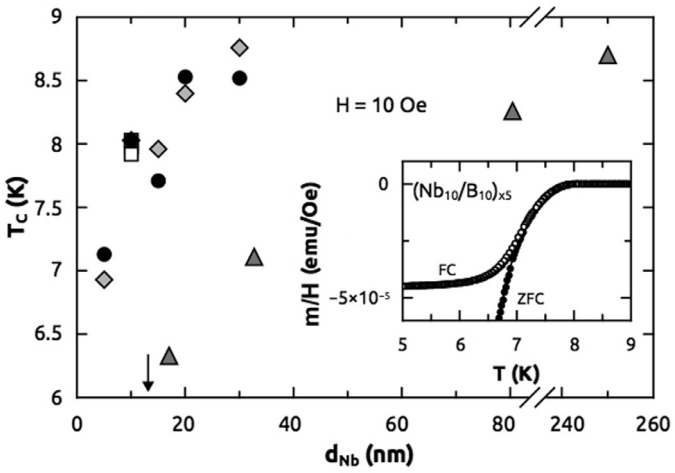

Fig. 3. Nb layer thickness, d_{Nb}, dependence of the superconducting transition temperature, T_c, defined as the onset of the diamagnetic magnetization at H = 10 Oe for Nb thin films and Nb/B superlattices. Vertical arrow: maximum thickness for non superconducting Nb thin films; triangles: Nb superconducting thin films; circles: Nbd_{Nb}Bd_B superlattices with $d_{Nb} = d_B$; diamonds: Nbd_{Nb}B10 superlattices; squares: Nb10Bd_B superlattices. The inset shows typical ZFC-FC magnetic moment curves at H=10 Oe.

very well, see inset to Fig. 1, resulting in $e = 16.9$ nm from the slope of the linear fit.

However, an anomaly that seems to be an intensity modulation is clearly present in Fig. 1 at around 2.25°. In order to understand its origin, we fit all the reflectivity data according to the recursive Parratt formalism [13] with Parratt32 program. [14] Fitting the data as a Nb single film over the Si substrate, dot line in Fig. 1, fails to describe the anomaly. Only when two additional oxide layers are included, a SiO_2 layer between the Nb film and the Si substrate, and a NbO_x layer at the Nb film surface, a good fit is obtained (continuous line in Fig. 1). The oxide layers come from the natural oxidation of the commercial Si wafers, and from the Nb oxidation in air after growth [15]. As a result of the fit, we obtained $e_{SiO_2} = 5.3$ nm, $e_{Nb} = 16.5$ nm and $e_{NbO_x} = 2.0$ nm for the layer thicknesses. Noticeably, the thickness of the Nb film is very similar to the value extracted from the data in Fig. 1 and Eq. (1), even when this equation neglects the presence of the oxide layers. In addition, the fit allowed us the estimation of δ. The δ value for the Nb film is 2.489×10^{-5}, which is similar to the expected theoretical value for bulk Nb of 2.4193×10^{-5} [10].

Fig. 2 shows the XRR data for $(Nb5/B5)_{\times 10}$ superlattice. Besides the Kiessig fringes, [11], seen as high-frequency small-intensity oscillations, the superlattice diffraction peaks are evident, following a law similar to Eq. (1) but with the period of the superlattice, Λ, in place of the thickness e. Similar behavior was also observed in the reflectivity measurements for all superlattices. The inset to Fig. 2 shows the superlattice peak position vs. order number. From the slope of a linear fit to these data we obtain $\Lambda = 11.1$ nm, in very good agreement with the expected periodicity, according to the deposition rates and deposition times.

Contrary to this good agreement in the peak positions, we were not able to obtain a good fit to the intensity data with the Parratt formalism [14]. Anyway, qualitative information regarding interface profile can be deduced from the intensity of the peaks. The observation of superlattice peaks in a $(Nb5/B5)_{\times 10}$ superlattice indicates an interface width smaller than 5 nm. Also, for an equal layer thickness of Nb and B, and very sharp interfaces, it is theoretically expected that the even order peaks have null intensity. These peaks are present, implying that one or both hypothesis are not correct. Since the periodicity obtained from the peak position is consistent with the intended one, we believe that the layer thickness is indeed approximately equal. The existence of these peaks could then indicate that the Nb and B layer thicknesses are not exactly equal, but most probably that the interfaces are not sharp, due to the presence of Nb-B compounds or interdiffusion.

3.2. Superconducting properties

The superconducting critical temperature of thin films and superlattices was defined as that of the onset of the diamagnetic signal for a small applied field of 10 Oe, see inset in Fig. 3. The evolution of T_c with Nb thickness for all the superlattices and also for Nb thin films is shown in Fig. 3. It is clear that for a given Nb thickness all superlattices show a higher T_c than a single Nb thin film.

Nb single films show superconductivity above 5 K for thicknesses above a critical thickness, which is between 12 and 17 nm. Superlattices T_c's are much less dependent from the Nb layer thickness, with superconductivity present down to $d_{Nb} = 5$ nm, which could be caused by the B layers acting as a protection for the oxidation of the Nb layers. Also, their T_c seems to be almost independent of the B-layer thickness. This may indicate that the Nb layers are decoupled from the superconducting point of view, with the superconducting order parameter being zero within the B layers [16]. Although the data presented here does not allow us to identify the mechanism, the Nb thickness dependence of T_c could have several microscopic origins: proximity effect between the Nb and B layers [16,17], intrinsic microscopic effects in the Nb layers [18,19], proximity and localization effects [20].

The superconducting transition was also studied through electrical transport measurements, see Fig. 4. All samples show a very sharp transition to zero resistance at T_c for $H = 0$. The transition width at zero field, defined between 20 and 80% of the normal state resistance above T_c, is $\lesssim$ 0.1 K. Residual Resistance Ratio (RRR) between room temperature and T_c is around 2 to 3.

Resistance (R) as a function of T was measured for the superlattices with H applied both perpendicular, $H_\perp$, or parallel, $H_\parallel$ to the sample surface, allowing for the determination of the perpendicular and parallel upper critical fields, $H_{c2\perp}(T)$ and $H_{c2\parallel}(T)$. Fig. 5 shows both critical fields for $(Nb10B10)_{\times 5}$ and $(Nb30B30)_{\times 3}$. The linear $H_{c2\perp}(T)$, in addition to the curved behavior for $H_{c2\parallel}(T)$, are in agreement with expectations for thin film with thickness, e smaller

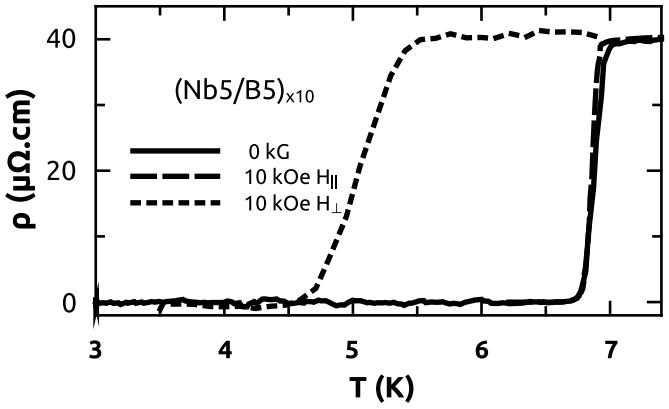

Fig. 4. Temperature dependence of the resistivity ρ for the $(Nb5/B5)_{\times 10}$ superlattice at zero field (continuous line), $H_{\parallel}$=10 kOe (dashed line) and $H_{\perp}$=10 kOe (dotted line).

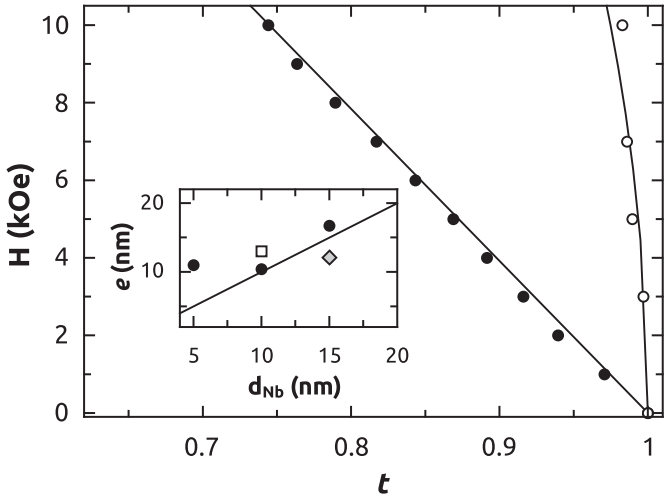

Fig. 5. Reduced temperature $t = T/T_c(H = 0)$ dependence of the upper critical fields $H_{c2\perp}$ (full symbols) and $H_{c2\parallel}$ (open symbols) for $(Nb10/B10)_{\times 5}$. Lines show fits to the data with Eqs. (2) and (3). The inset shows the thickness e obtained from Eq. (3) vs. the nominal Nb thickness for $(Nbd_{Nb}/Bd_B)_{\times N}$ with $d_{Nb} = d_B$ = 5, 10, 15 and 30 nm (black circles), $(Nbd_{Nb}/B10)_{\times N}$ with d_{Nb} = 15 and 30 nm (gray diamonds) and $(Nb10/B5)_{\times 6}$ (white square). The solid line indicates $e = d_{Nb}$.

than the superconducting coherence length, $\xi(T)$:

$$H_{c2\perp}(T) = \frac{\phi_o}{2\pi\xi^2(0)}(1-t) \tag{2}$$

$$H_{c2\parallel}(T) = \frac{\phi_o\sqrt{12}}{2\pi e\xi(0)}(1-t)^{1/2} \tag{3}$$

where $\phi_o = 2.07 \times 10^{-7}$ Oe.cm^2 is the flux quantum and $t = T/T_c(H = 0)$. Fitting the data with these expressions we consistently obtained the value $\xi(0) \approx 10$ nm, typical for our sputtered Nb films, [21] and e of the order of the Nb layer thickness, instead of the total superlattice thickness ($\approx$ 100 nm), see inset to Fig. 5. This confirms the superconducting decoupling of the Nb layers, implying that the superlattice should be considered as a stacking of independent Nb films of thickness d_{Nb}.

Fig. 6 presents the estimation of the critical current for the $(Nb30/B30)_{\times 3}$ superlattice. This was calculated from the irreversible part of the magnetization using Bean's model, [22] $J_c = k\Delta M(H)/w[1-(w/3l)]$, where $k = 20$ A.cm^2/emu, w is the width and l the length of the sample ($w < l$), and $\Delta M(H)$ is the difference between the upper and lower branches of the magnetization in a hysteresis loop, see inset to Fig. 6. [23] The J_c values ranging

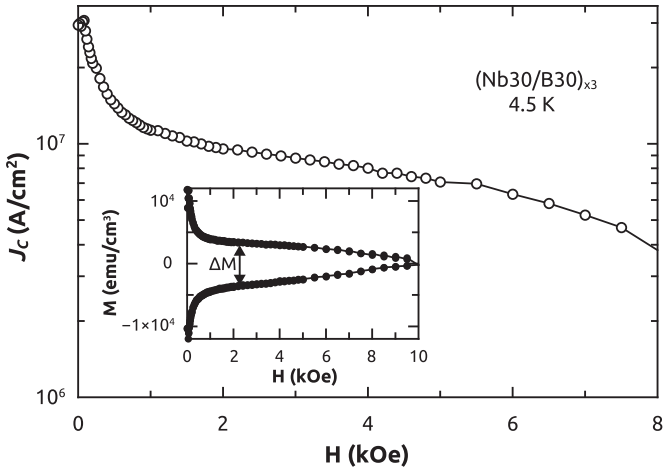

Fig. 6. Field dependence of the critical current J_c at 4.5 K for the superlattice $(Nb30/B30)_{\times 3}$. Data are obtained from magnetization vs. magnetic field curves (inset) through Bean's model, see text.

10^7 A/cm^2 are promising for the use of this material in a TES design.

4. Conclusions

We have studied the Nb/B superlattice system due to its possible use in neutron detection TES. We show that it is possible to reduce the thicknesses of the Nb film down to 5 nm retaining a superconducting transition. In contrast the Nb films present no transition down to 5K for thicknesses below a critical one between 12 and 17 nm. Besides, we found that the critical temperature for the superlattices depends to some extent on the Nb layer thickness, allowing the possibility of tunning the T_c from $\sim$ 8.5 K down to an appropriate value given by the refrigeration system intended for the cryogenic cooling. From the superconducting point of view, the superlattices behave as a stack of independent Nb films with thickness d_{Nb}. In conclusion we find that Nb/B superlattice system is a very good candidate for a neutron transition edge detector, as it combines a superconducting element with B maintaining a sharp superconducting transition.

5. Acknowledgments

Work partially supported by grants 06/C441 from SECTyP-Univ. Nac. Cuyo, and PICT 2012-0770 from FONCyT. D.G.F. thanks CONICET for support through a posdoctoral scholarship. N.S. acknowledges financial support from the ExploÆ'ra Sup program of the Rhône-Alpes region, France.

References

[1] G.F. Knoll, Radiation Detection and Measurement, third, John Wiley & Sons, Inc., 2000.
[2] P.K. Day, H.G. LeDuc, B.A. Mazin, A. Vayonakis, J. Zmuidzinas, A broadband superconducting detector suitable for use in large arrays, Nature 425 (6960) (2003) 817–821, doi:10.1038/nature02037. http://www.nature.com/doifinder/10.1038/nature02037.
[3] J. Nagamatsu, N. Nakagawa, T. Muranaka, Y. Zenitani, J. Akimitsu, Superconductivity at 39 k in magnesium diboride, Nature 410 (2001) 63–64.
[4] T. Ishida, D. Fujiwara, M. Nishikawa, Superconducting MgB 2 films as radiation detectors, J. Korean Phys. Soc. 48 (5) (2006) 1026–1031, doi:10.3938/jkps.48.1026.
[5] I. Yagi, N. Yoshioka, H. Shishido, T. Yotsuya, S. Miki, Z. Wang, T. Ishida, Current-biased transition edge detector of mgb2 nanowires for nneutron: imaging by scanning laser, IEEE Trans. Appl. Supercond. 23 (3) (2013) 2200904.
[6] N. Yoshioka, Y. Narukami, S. Miyajima, H. Shishido, A. Fujimaki, S. Miki, Z. Wang, T. Ishida, Four-channel current-biased kinetic inductance detectors using mgb2 nanowires for sensing pulsed laser irradiation, J Low Temp Phys 176 (2014) 273–278.

[7] , Binary Alloy Phase Diagrams, in: T.B. Massalski, H. Okamoto, P.R. Subramanian (Eds.), ASM International, 1990.
[8] T. Ishida, N. Yoshioka, Y. Narukami, H. Shishido, S. Miyajima, A. Fujimaki, S. Miki, Z. Wang, M. Hidaka, Toward mega-pixel neutron imager using current-biased kinetic inductance detectors of nb nanowires with 10b converter, J Low Temp Phys 176 (2014) 216–221.
[9] T. Ishida, S. Miyajima, Y. Narukami, N. Yoshioka, H. Shishido, M. Hidaka, A. Fujimaki, Toward neutron radiography using two arrays of Nb-based current-biased kinetic inductance detectors with 10B converter sandwiched in-between, IEEE Trans. Appl. Supercond. 25 (3) (2015) 2401304, doi:10.1109/TASC.2014.2383394. http://ieeexplore.ieee.org/lpdocs/epic03/wrapper.htm?arnumber=7051246.
[10] B.L. Henke, E.M. Gullikson, J.C. Davis, X-ray interactions: photoabsorption, scattering, transmission, and reflection at e = 50–30.000 ev, z = 1–92, At. Data Nucl. Data Tables 54 (1993) 181–342.
[11] H. Kiessig, Interferenz von röntgenstrahlen an dünnen schichten, Ann. Phys. 402 (7) (1931) 769–788, doi:10.1002/andp.19314020702. http://doi.wiley.com/10.1002/andp.19314020702.
[12] E.E. Fullerton, I.K. Schuller, H. Vanderstraeten, Y. Bruynseraede, Structural refinement of superlattices from x-ray diffraction, Phys. Rev. B 45 (16) (1992) 9292–9310, doi:10.1103/PhysRevB.45.9292. http://link.aps.org/doi/10.1103/PhysRevB.45.9292.
[13] L.G. Parratt, Surface studies of solids by total reflection of X-Rays, Phys. Rev. 95 (2) (1954) 359–369, doi:10.1103/PhysRev.95.359. http://link.aps.org/doi/10.1103/PhysRev.95.359.
[14] C. Braun, Parratt32 -or The Reflectivity Tool-, version 1.6.0 build 242, 1997–2002, HMI Berlin.
[15] A. Gibaud, D.F. McMorrow, P.P. Swaddling, Determination of the X-ray scattering lineshape from a Nb thin film using synchrotron radiation, J. Phys. 7 (14) (1995) 2645. http://stacks.iop.org/0953-8984/7/i=14/a=005.
[16] P.G. De Gennes, Boundary effects in superconductors, Rev. Mod. Phys. 36 (1) (1964) 225–237, doi:10.1103/RevModPhys.36.225. http://link.aps.org/doi/10.1103/RevModPhys.36.225.
[17] K. Yoshii, H. Yamamoto, K. Saiki, A. Koma, Superconductivity and electrical properties in single-crystal ultrathin nb films grown by molecular-beam-epitaxy, Phys. Rev. B 52 (18) (1995) 13570.
[18] A.F. Mayadas, Electrical characteristics of rf-sputtered single-crystal niobium films, J. Appl. Phys. 43 (3) (1972) 1287, doi:10.1063/1.1661258. http://scitation.aip.org/content/aip/journal/jap/43/3/10.1063/1.1661258.
[19] S. Bose, P. Raychaudhuri, R. Banerjee, P. Vasa, P. Ayyub, Mechanism of the size dependence of the superconducting transition of nanostructured nb, Phys. Rev. Lett. 95 (2005) 147003, doi:10.1103/PhysRevLett.95.147003. http://link.aps.org/doi/10.1103/PhysRevLett.95.147003.
[20] S.I. Park, T.H. Geballe, Tc depression in thin nb films, Phys. B 135B (1985) 108–112.
[21] G. Grinblat, Susceptibilidad Magnetica Alterna y Transporte Electrico en Superredes de Nb/Co, Instituto Balseiro, CNEA and Univ. Nac. de Cuyo, Argentina, 2010 Master thesis.
[22] C.P. Bean, Magnetization of hard superconductors, Phys. Rev. Lett. 8 (6) (1962) 250–253.
[23] E.H. Brandt, Superconductors of finite thickness in a perpendicular magnetic field: strips and slabs, Phys. Rev. B 54 (6) (1996) 4246–4264.